Supporting Information

Mn-doped Atomic SnO_2 Layers for Highly Efficient CO_2 Electrochemical Reduction

Yajuan Wei,[1] Jia Liu,[2] Fangyi Cheng,[1] Jun Chen[1]*

[1] Key Laboratory of Advanced Energy Materials Chemistry (Ministry of Education), Renewable Energy Conversion and Storage Center, College of Chemistry, Nankai University, Tianjin 300071, China

[2] Department of Chemistry, School of Science, Tianjin University, Tianjin 300072, China.

E-mail: chenabc@nankai.edu.cn

1. Materials and Methods

Preparation of TMO. In a typical synthesis, 150 mg of $Mn(NO_3)_2{\cdot}4H_2O$ was firstly dissolved in 10 mL dried methyl alcohol by ultrasonic for 3 minutes. Then, 220 mg of anhydrous $SnCl_2$ was added in the settled solution for ultrasonic 10 minutes until all the grains dissolved. After that, the above mixture was transferred into a 20 mL glass bottle, and heated at 120 ^oC for 2 hours by using oven. Then, the obtained white powder was calcinated at 200 ^oC for 5 hours in the muffle furnace and after that the powder was washed by methanol to remove Cl^- anions and unreacted dissolvable salts. Finally, the obtained white powders were dried in vacuum oven at 120 ^oC for 3 h. The other two catalysts TMO-1 and TMO-2 (Sn/Mn ratios 1:1 and 5:1, respectively) were obtained in the same way. Three molar ratios of Sn/Mn precursors were considered. When the mole ration of Sn/Mn is 3:2, the obtained TMO catalyst exhibits the best performance of CO_2RR (Figure S14). Therefore, the discussion and main characterization were focused on TMO.

Preparation of SnO_2. The commercial SnO_2 purchased from Xien Si BioChem Tech. Co. Ltd was calcinated at 200 ^oC for 6 hours in air to make sure the only exist of Sn(IV).

Preparation of $Mn(OH)_2$. Add over mass of $NH_3{\cdot}H_2O$ to $MnCl_2$ solution in a plastic self sealed pocket to prevent sample from contacting with air. The obtained white precipitant was directly used in XAFS test.

Catalysts characterizations. Powder X-ray diffraction (XRD) patterns were obtained on a Rigaku MiniFlex600 diffractometer with Cu Kα radiation (λ=0.154nm, 40kV and 15 mA). The scan speed was 4°/min^{-1} and the step was 0.02°. The scanning electron microscope (SEM) images were obtained by JEOL JSM-7500F. High-resolution transmission electron (HRTEM) images were carried out by Tecnai G2 F20. HADDF-STEM images were recorded by Titan Cubed Themis G2300 working at 200 kV. Atomic force microscope (AFM) images were measured by Bruker icon. Inductively coupled plasma optical emission spectrometry (ICP-OES) was tested by Agilent 725ES. Photoemission spectroscopy experiments (XPS) spectra were collected on ESCALAB 250xi with Al Kα as source gun type. Nuclear magnetic resonance (NMR) were tested by Brook ASCEND400. CO_2 adsorption experiment were carried out on the surface area analyzer Micromeritics (ASAP 2020) purchased from quantum chrome USA.

Calculation of near zero coverage isosteric heat. CO_2 adsorption experiment were carried out on the surface area analyzer Micromeritics (ASAP 2020) at 273K and 298K, respectively. The near zero coverage isosteric heat (Q_{st}) of

CO_2 on TMO calculated based on Clausius–Clapeyron relation, where *p* is the pressure, *T* is the temperature (K), and *R* is the gas constant (8.314 J mol^{-1} K^{-1}).

$$\ln\frac{p_2}{p_1} = \frac{Qst}{R}\left(\frac{1}{T_1} - \frac{1}{T_2}\right)$$

XAFS measurements and analysis. The Sn L3-edgs and Mn K-edgs XAFS were measured at Singapore Synchrotron Light Source. The light Source provides a wide energy range of 1.2 -12.8 keV with a resolving ~ 3.8×10^{-4}@ 8 KeV. The NEXAFS measurement was performed in a vacuum and atmosphere of pure CO_2 under 1 atm at room temperature. The powder sample was compress into tablet for test. Mn metal foil was used to calibrate the beam line energy.

Electrochemical measurements. The CO_2 electrocatalytic reduction were applied by a three-electrode system with a proton exchange membrane Nafion 117 as a separator in a custom-designed gas tightness H-type electrochemical cell with a circulating water layer at an electrochemical station (CHI660E). 20 mg powders including 12 mg TMO catalyst and 8 mg Carbon Vulcan 72 were grinded fully and then with 40 µL Nafion solution (5 wt%) were dispersed in 1ml water-ethanol solution (with a volume ration of 3:1) to form a homogeneous ink by sonicating for at least 1 hour. The resulting suspension was then dropped on a 1*1 cm Toray carbon paper (Toray TGP-H-060, Toray Industries Inc.) until a catalyst loading of 1 mg cm^{-2} and dried naturally to be used as the working electrode. The silver chloride electrode (Ag/AgCl) and platinum wire electrode were served as reference and counter electrode, respectively. Each compartments of the H-type electrochemical cell contains 65 ml 0.1M $KHCO_3$ electrolyte, and nearly 35 ml headspace for collecting generated gases. In the cathode compartment, the products H_2 and CO were regularly vented into the gas sampling loop of Gas chromatography for online analysis, otherwise the product O_2 in anode compartment was vented out from the exit. Before CO_2 reduction experiment, the 0.1M $KHCO_3$ electrolyte was pre-saturated with CO_2 (99.999%) at a flow rate of 15 mL/min for 30 minutes until saturated (pH=6.8). The reference potentials in this study converted to RHE as follows:

E (vs. RHE) = E (vs. Ag/AgCl) + 0.210 V+0.0591×pH

All the potentials were iR-compensation by 85%. The electrolyte in the cathode compartment was stirred at a rate of 1000 rpm. In a typical procedure, LSV with a scan rate of 15 mv/s was collected in both of Ar (99.999%) or CO_2 (99.999%) pre-saturated 0.1M $KHCO_3$ for comparison. Electrolysis was applied for 1.5 h at each selected potential. The temperature of circulating water is constant of 25 ^{o}C.

The products analysis includes two parts. The gaseous products were detected online by gas chromatograph (GC, Shimadzu 2010 plus) which equipped with a ShinCarbon ST micropacked columns, 50 µL sample loop and the BID detector that can analyzed for H_2 and CO. Ultra pure helium (＞99.9999%) was carrier gas. The test processes were applied by temperature programming method to separate H_2 and CO.

The liquid product formic acid was analyzed and quantified by nuclear magnetic resonance spectroscopy (NMR, Bruker ASCEND400), in which 0.5 mL electrolyte was added with 0.1 mL D_2O and 190 ppm (m/m) dimethyl sulfoxide as an internal standard. The molar quantities of formic acid (n_{HCOOH}) were obtained by standard curve method. The Faradic efficiency of formic acid (FE_{HCOOH}) was calculated as follows: $FE_{HCOOH} = 2F\times n_{HCOOH} / Q$, where F is the Faradic constant and Q is calculated by integral area of Amperometric-T (i-t) Curves.

DFT Calculation. During DFT calculations, Perdew-Burke-Ernzerhof (PBE) exchange-correlation functional were used with a plane wave pseudopotential implementation.[1] The kinetic energy cutoff was set to 340 eV. A Hubbard

U term was added to the PBE functional to describe the localized 3d electrons in Mn and Sn. For Mn, a value of Ueff = 4.5 eV was used on its d orbital. The model was a periodic slab with a (2×2×3) surface unit cell. The vacuum gap of 15 Å was set. A (2×2×1) Gamma k-point was adopted. The atoms and top atomic layers of the slab were completely relaxed to obtain accurate adsorptive configuration, while other bottom layers were froze to their bulk position.

A periodic SnO_2 (001) surface slab with 2×2 arrangement was used for calculation. One of Sn atom was substituted by Mn(II) and generate a oxygen vacancy in unit cell. When calculated free energy for each transition state as $\Delta G=\Delta E_0 -\Delta ZPE+\int\Delta C_p dT-T\Delta S$, where ΔG is the free energy change, ΔE_0 is the energy change of each state calculated at 0 K. ΔZPE is the variation in zero point energies (ZPE). C_p is heat capacity of each component. ΔS is the entropy change of the reaction. Entropy and C_p value of each state was obtained by vibration analysis. The proton-electron pair (H^++e) was assumed and the corresponding energy was expressed using the reversible hydrogen electrode (RHE) [2, 3].

2. Supplementary Figures and Tables

Table S1. the amount of doped Mn.

Sample	TMO	TMO-1	TMO-2
Mn (wt%)	11.86	16.25	5.53

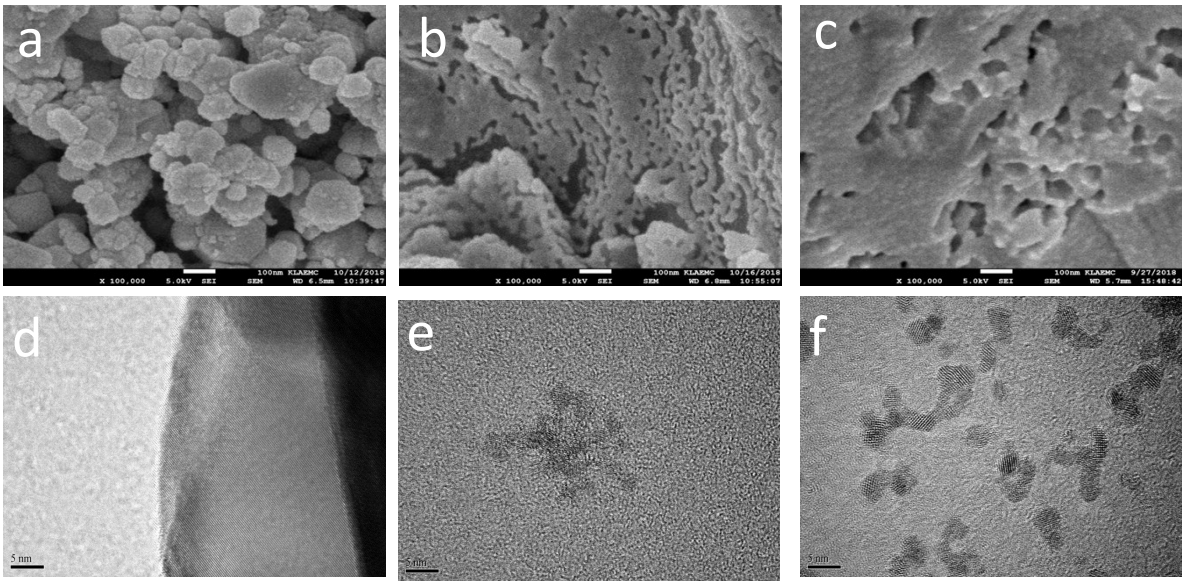

Figure S1. SEM and HRTEM images of catalysts. (a, d) commercial SnO_2; (b, e) TMO-1; (c, f) TMO-2

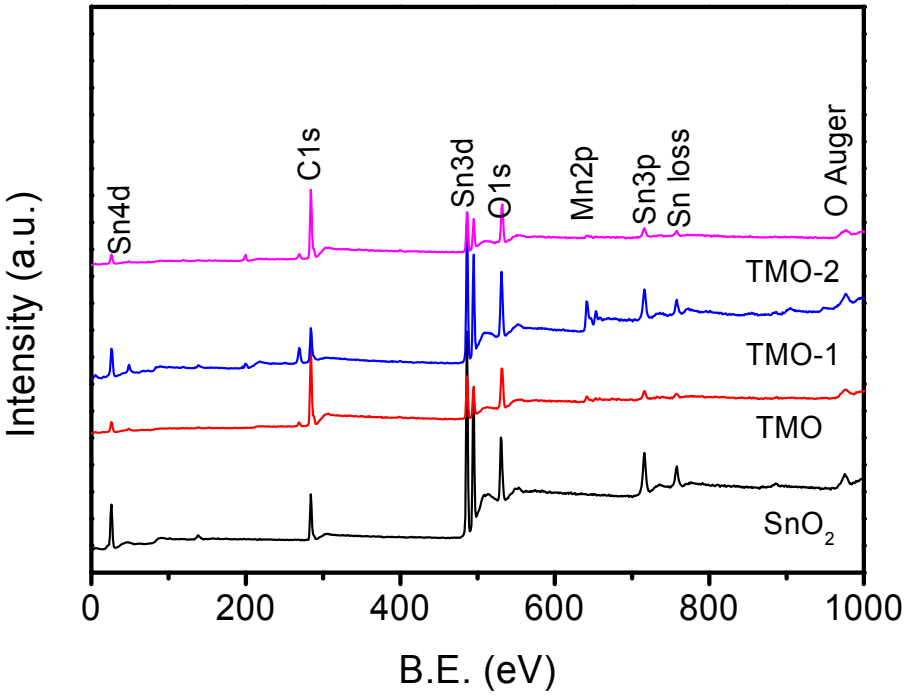

Figure S2. XPS survey spectra of commercial SnO_2, TMO, TMO-1, and TMO-2.

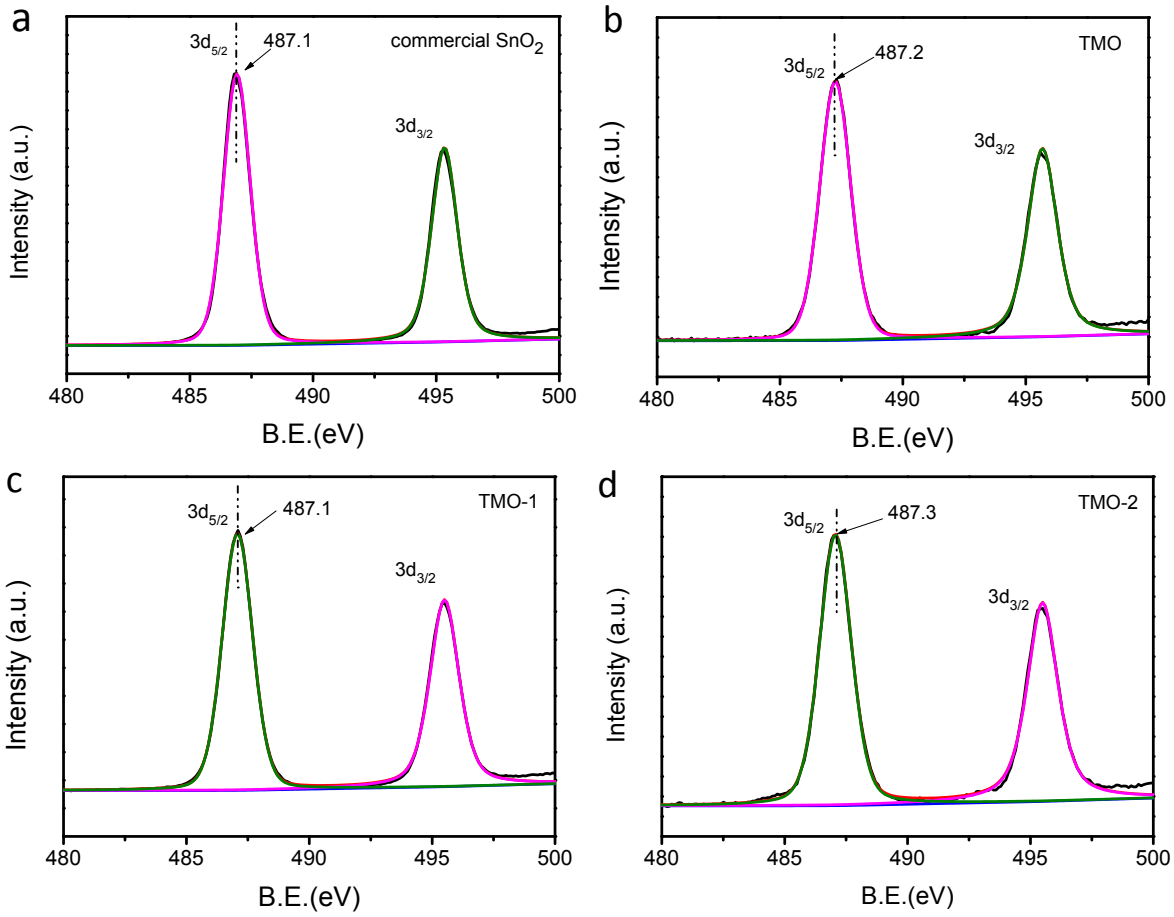

Figure S3. XPS of Sn 3d of catalysts.

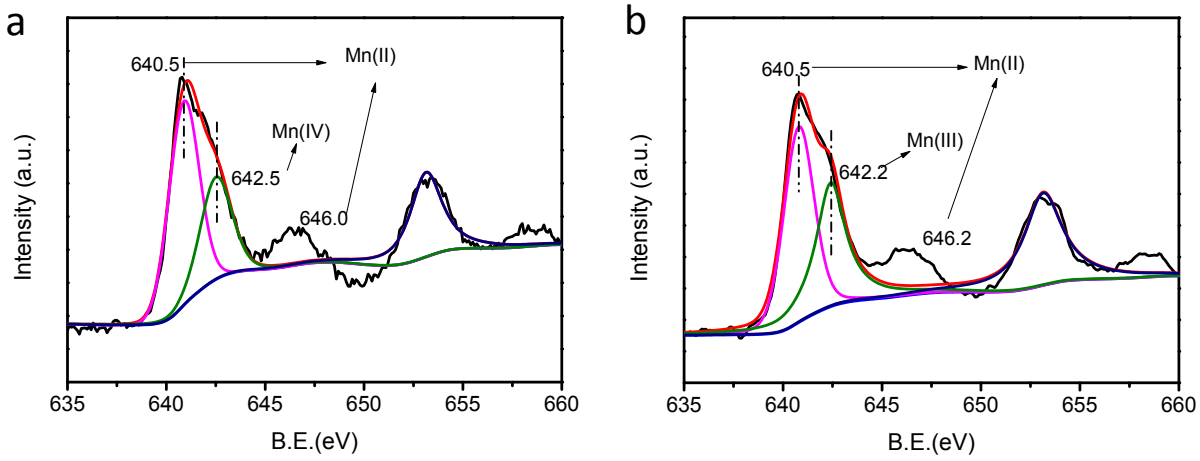

Figure S4. XPS of Mn2p of catalysts (a: TMO-1; b: TMO-2)

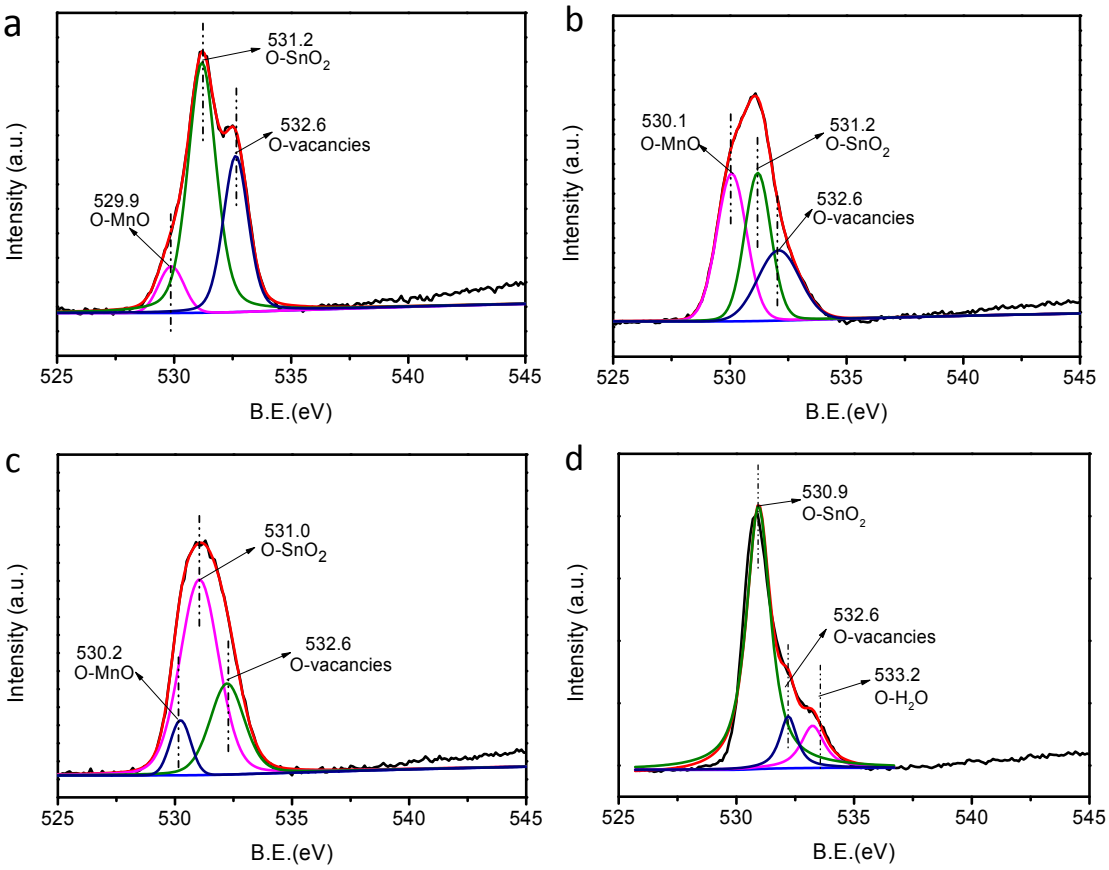

Figure S5. XPS of O1s of catalysts. (a:TMO; b:TMO-1; c: TMO-2; d: commercial SnO_2)

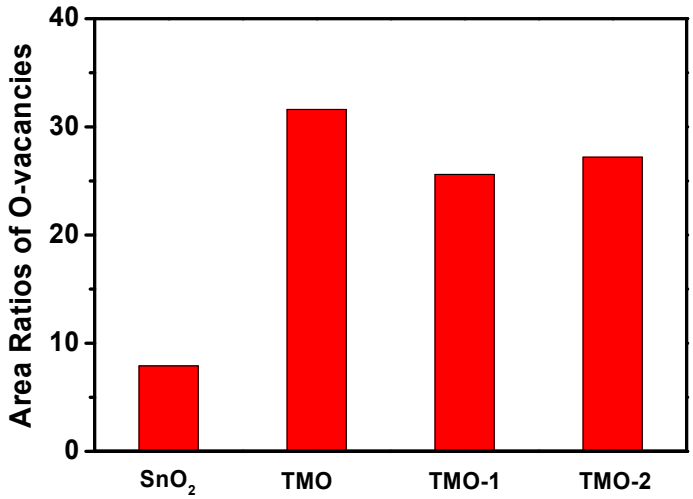

Figure S6. The calculated ratio of integral areas for the peaks located at ~530 eV, ~531eV and 532.6 eV in O 1s XPS spectra of different catalysts.

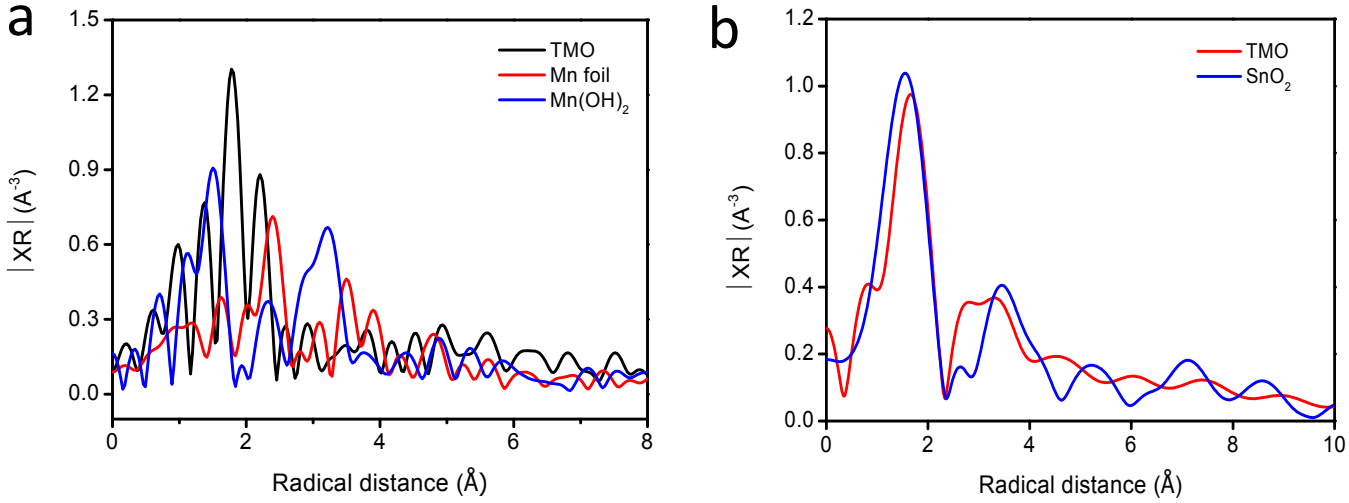

Figure S7. (a) Mn K-edge Fourier transformed EXAFS spectra in R space; (b) Sn L3 edge Fourier transformed EXAFS spectra in R space.

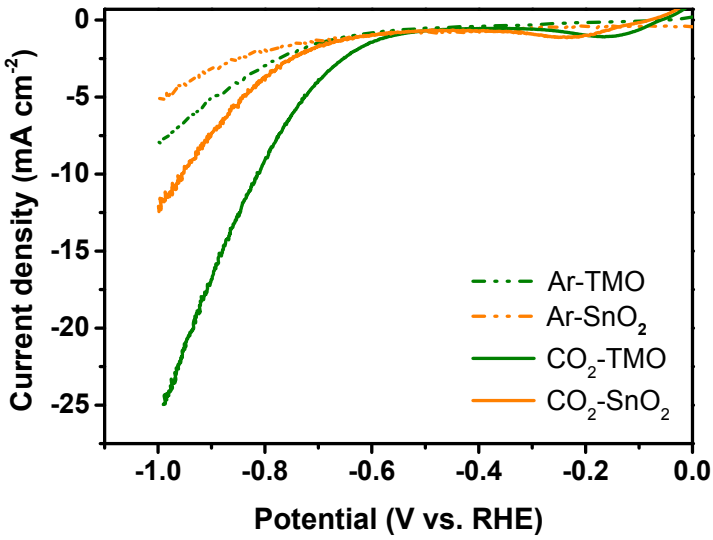

Figure S8. Comparison of LSV in CO_2-saturated and Ar-saturated 0.1 M $KHCO_3$ aqueous solution.

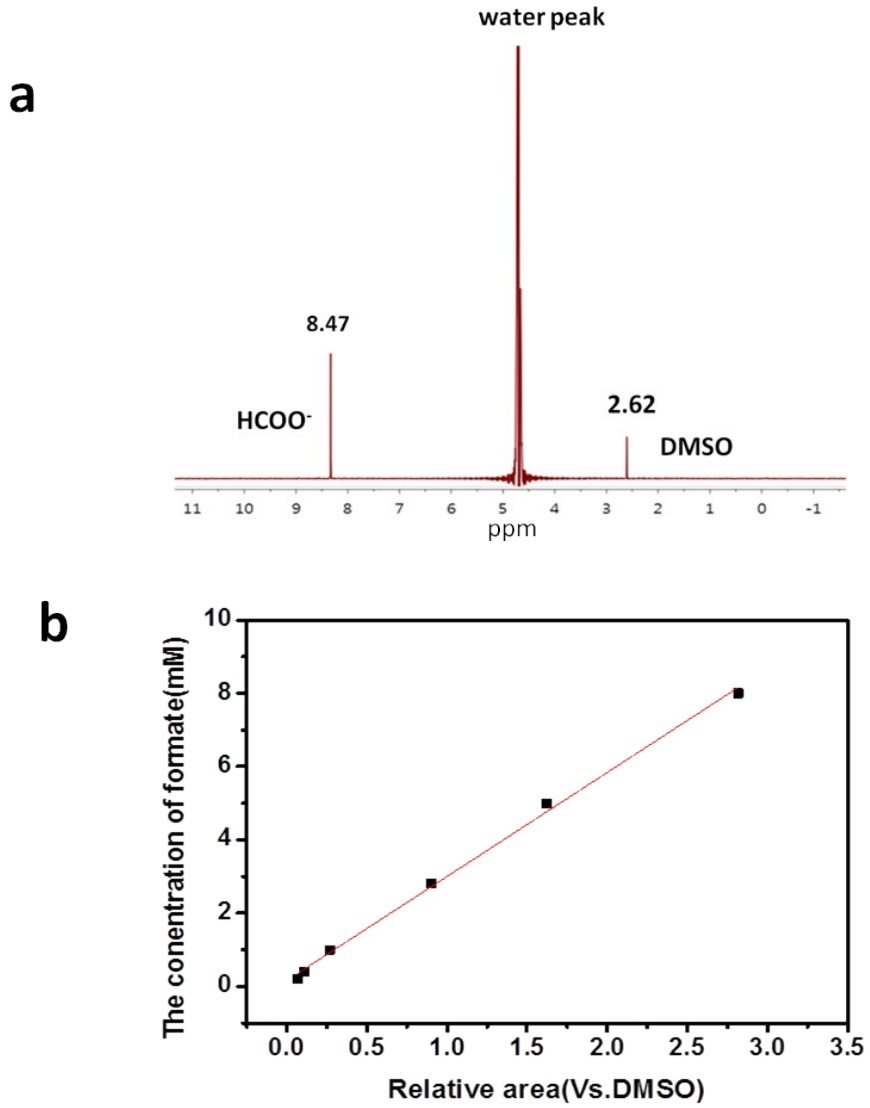

Figure S9 a) ^{1}H-NMR spectrum of the electrolyte after 1.5 h electrolysis at -0.83 V (vs. RHE) of TMO. (The ^{1}H-NMR spectrum for formic acid determination by pre-saturation water suppression); b) Linear relationship between formic acid concentration and relative area (Vs. DMSO).The standard curve was obtained as follows: 0.5 mL of formic acid solution with different concentration from 0.2 mM to 8 mM was mixed with 0.1 mL D_2O/DMSO solution (DMSO was 190 ppm) as an internal standard.

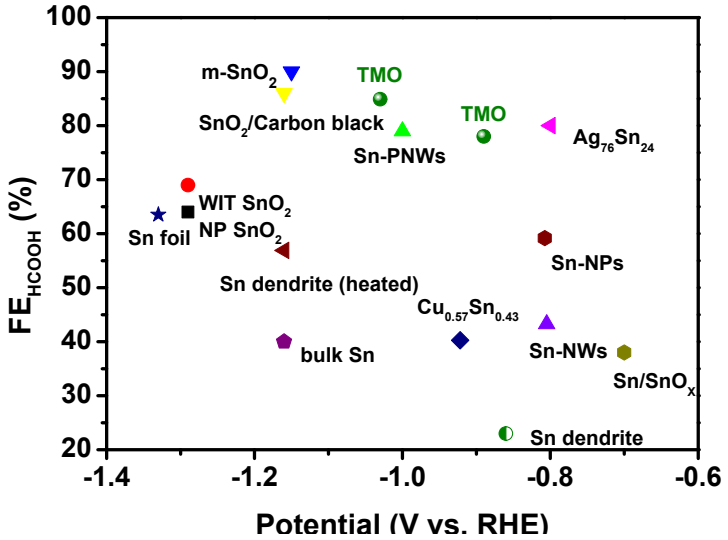

Figure S10. Comparison of FE_{HCOOH} for Sn-based catalysts (details summarized in supplementary Table S2)

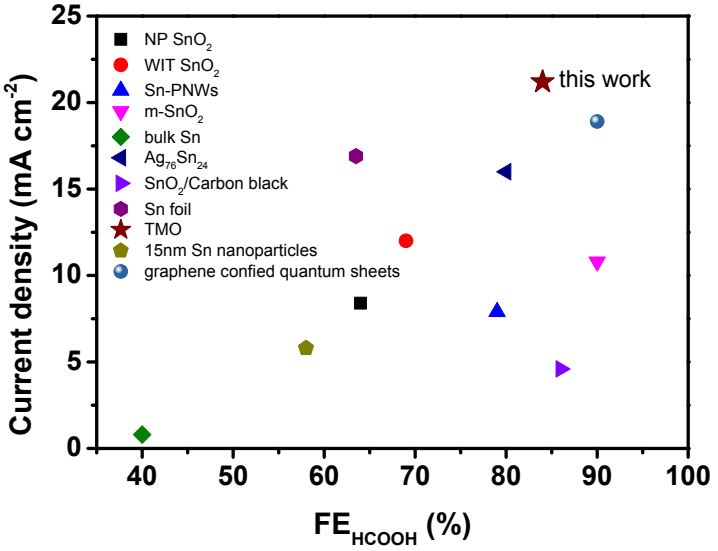

Figure S11. Comparison of j_{HCOOH} for Sn-based catalysts and noble metals. (details summarized in supplementary Table S2)

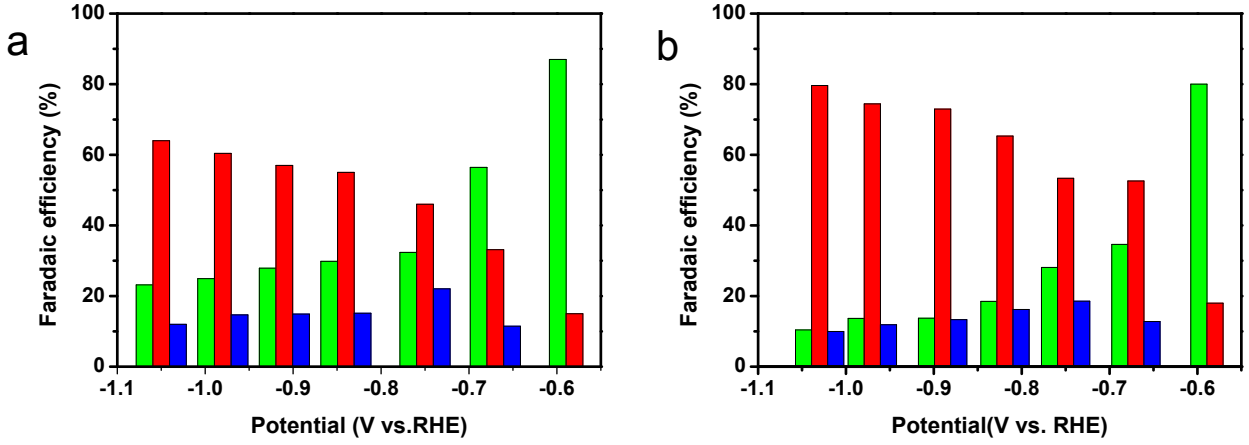

Figure S12. Products Faradaic efficiency of (a) TMO-1 and (b) TMO-2. (red bar: HCOOH; blue bar: CO; green bar:H_2)

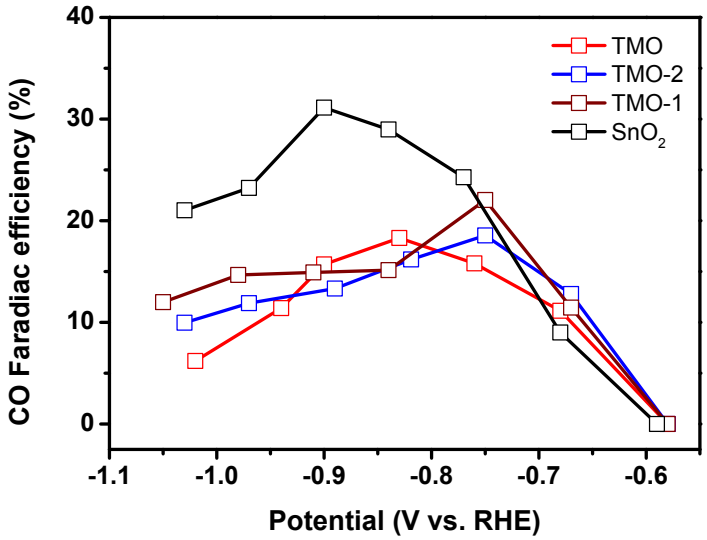

Figure S13. Comparison of CO Faradaic efficiency of catalysts.

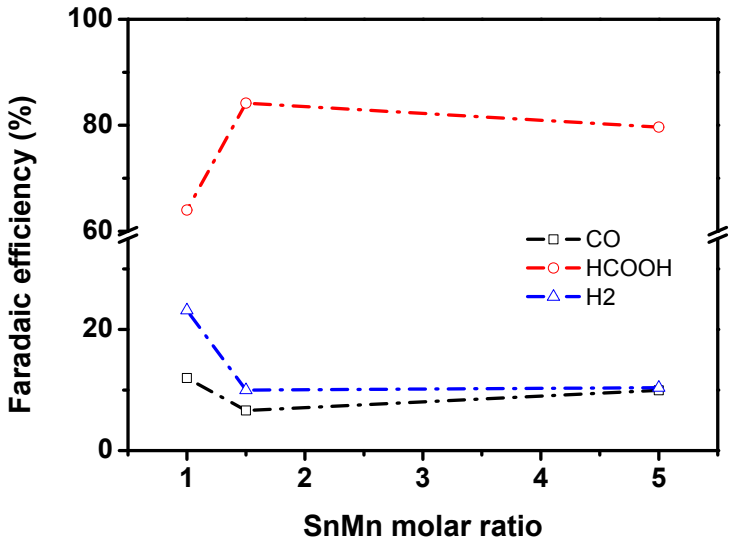

Figure S14. Products Faradaic efficiency of different Sn/Mn molar ratios when applied on -1.0 V vs.RHE.

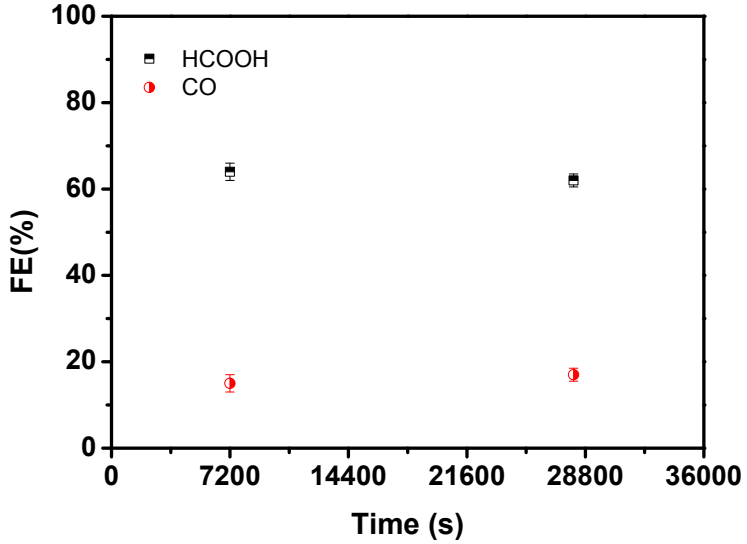

Figure S15. Faradaic efficiency of HCOOH and CO during CO_2RR stability test of TMO at -0.83 V (vs.RHE).

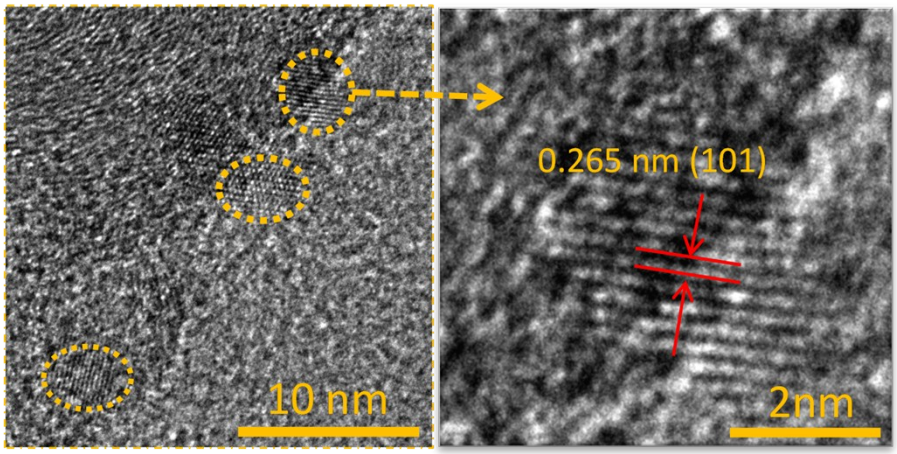

Figure S16. TEM images of TMO after stability test. (The TMO nanosheet still exhibits ~5nm and the (101) lattice of SnO_2 were observed.)

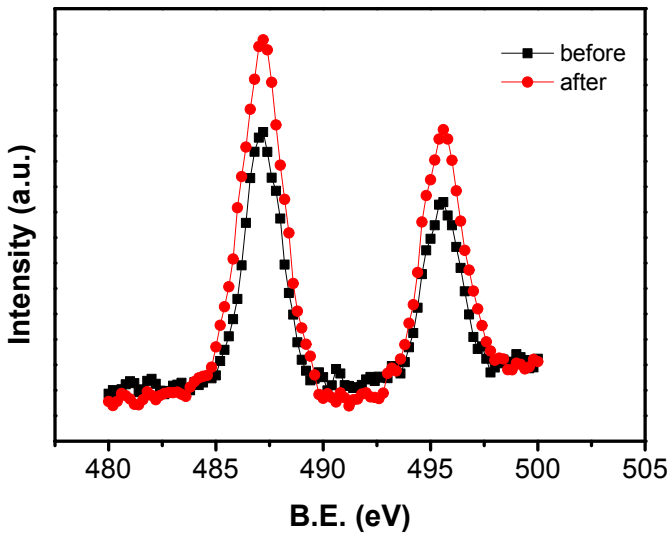

Figure S17. Comparison of Sn 3d XPS spectrum of TMO before and after stability test.

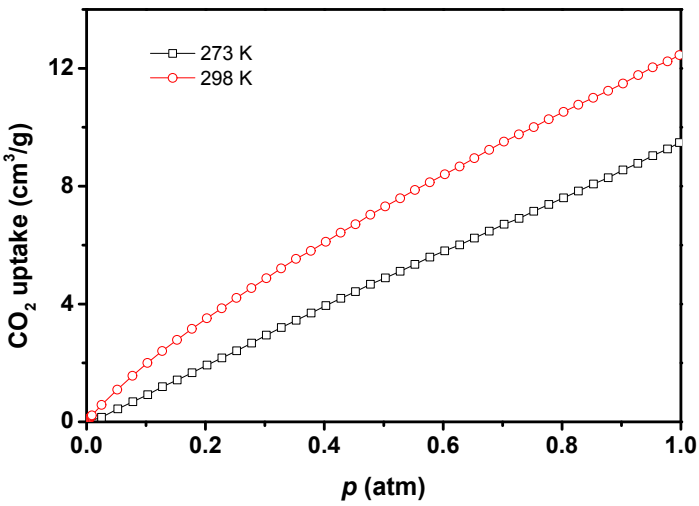

Figure S18. CO_2 adsorptive isotherm curves at 273 K and 298K.

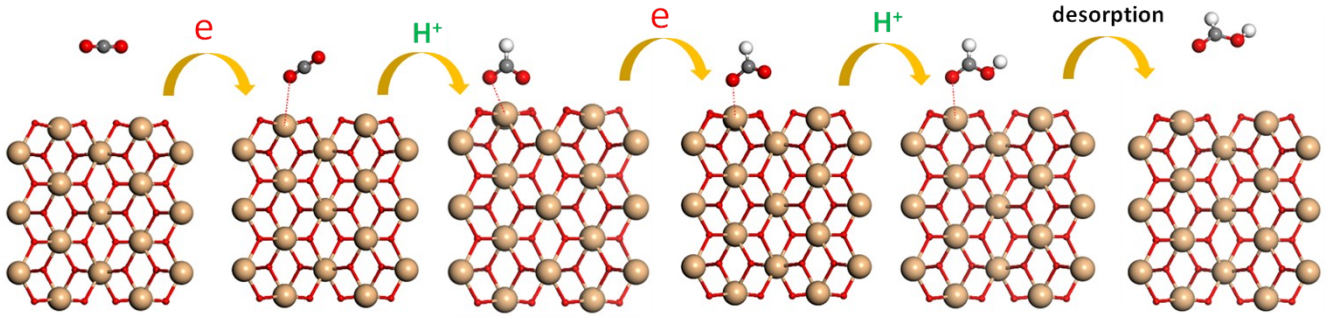

Figure S19. DFT study of formic acid formation process on SnO_2 surface.

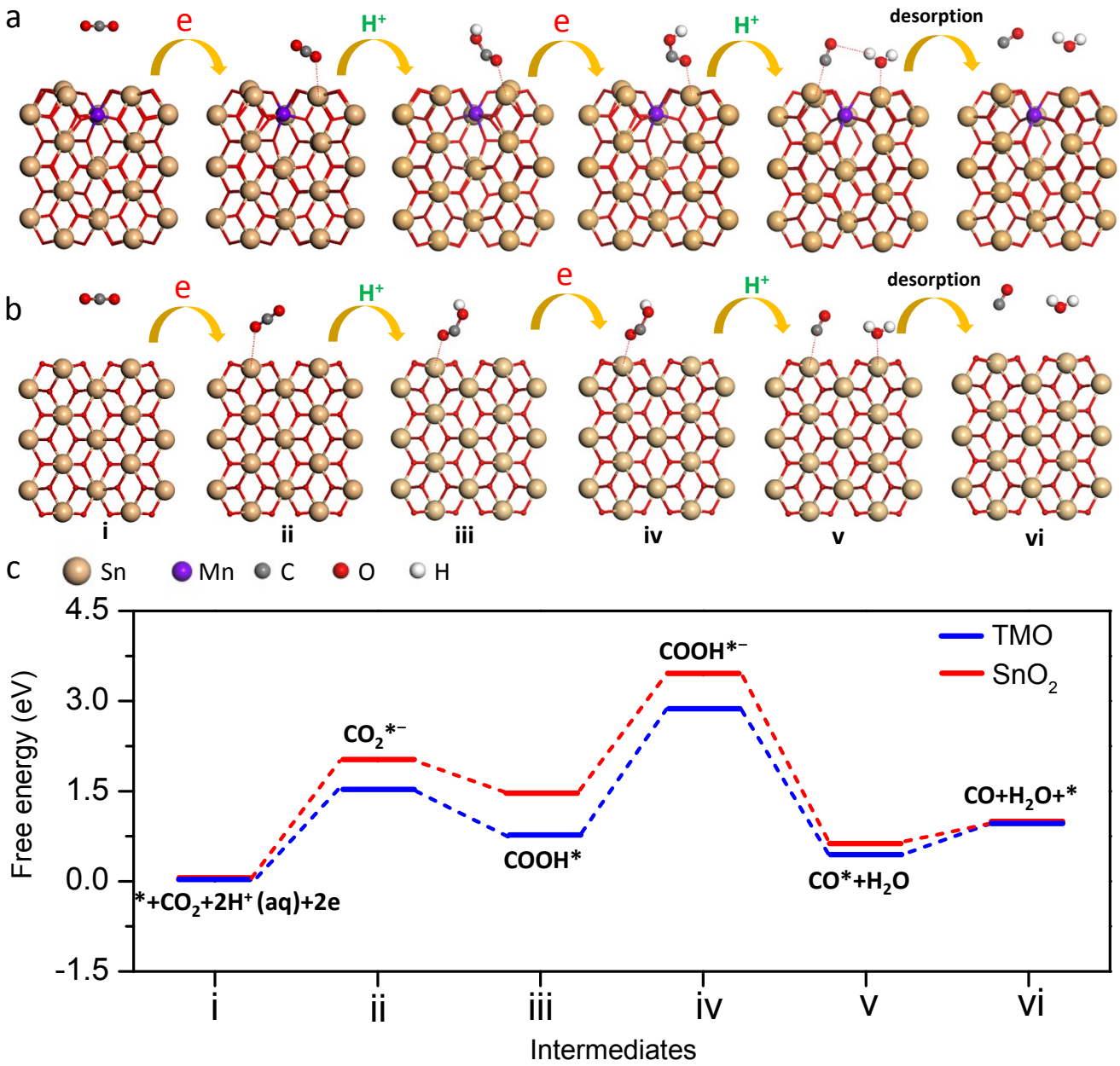

Figure S20. DFT study of CO formation process. (a) Optimized structure of main intermediates on TMO surface. (b) Optimized structure of main intermediates on SnO_2 surface. (c) Free energy diagram of each step. * indicate active sites on the surface and adsorbed species.

Table S2. Comparison of formic acid selective catalysts.

catalyst	electrolyte	applied potential (V vs. RHE)	j_{HCOOH} (mA cm^{-2})	FE_{HCOOH} (%)	onset potential (V vs.RHE)	Catalyst loading(mg cm^{-2})	References
NP SnO_2	0.1M $KHCO_3$	-1.29	8.4	64	-0.99	1	[4]
WIT SnO_2	0.1M $KHCO_3$	-1.29	12	69	-0.69	1	[4]
Sn-pNWs	0.1M $KHCO_3$	-1.00	~7.9	79	-0.55	4	[5]
Sn-NPs	0.1M $KHCO_3$	-0.8	~1	58	-0.6	4	[5]
Sn dendrite	0.1M $KHCO_3$	-0.86	~1.2	23	-0.56	-	[6]
Sn dendrite (heated)	0.1M $KHCO_3$	-1.06	~6.48	59	-0.56	-	[6]
m-SnO_2	0.1M $KHCO_3$	-1.15	10. 8	90	-0.55	1	[7]
commericial Bi	0.5M $NaHCO_3$	-0.81	2	95	-0.66	1	[8]
BiNs	0.5M $NaHCO_3$	-1.01	17	95	-0.56	1	[8]
bulk Sn	0.1M $NaHCO_3$	-1.16	0.8	40	-0.46	0.2	[9]
15 nm Sn nanoparticles	0.1M $NaHCO_3$	-1.16	5.8	58	-0.46	0.2	[9]
graphene confined Sn quantum sheets	0.1M $NaHCO_3$	-1.16	18.9	90	-0.46	0.2	[9]
$Cu_{0.57}Sn_{0.43}$	0.05M $KHCO_3$	-0.9	1.43	40	-0.4	-	[10]
$Ag_{76}Sn_{24}$	0.5M $NaHCO_3$	-0.80	16	80	-0.49	1	[11]
Sn/SnO_x	0.5M $NaHCO_3$	-0.7	~0.68	38	-0.5	-	[12]
Sn foil	0.5M $KHCO_3$	-1.33	16.9	63.5	-	-	[13]
SnO_2/carbon black	0.1M $NaHCO_3$	-1.16	4.6	86	-0.34	0.2	[14]
SnO_2/graphene	0.1M $NaHCO_3$	-1.16	9.5	93	-0.59	0.2	[14]
TMO	0.1M $KHCO_3$	-1.03	21.2	85	-0.49	1	this work
Commercial SnO_2	0.1M $KHCO_3$	-1.05	11	61	-0.79	1	this work

References

1. J. P. Perdew, K. Burke and M. Ernzerhof, *Phys. Rev. Lett.*, 1996, **77**, 3865-3868.
2. J. K. Nørskov, J. Rossmeisl, A. Logadottir, L. Lindqvist, J. R. Kitchin, T. Bligaard and H. J. K. Jonsson, *J. Phys. Chem. B*, 2004, **108**, 17886-17892.
3. Q. Li, J. Fu, W. Zhu, Z. Chen, B. Shen, L. Wu, Z. Xi, T. Wang, G. Lu, J. J. Zhu and S. Sun, *J. Am. Chem. Soc.*, 2017, **139**, 4290-4293.
4. L. Fan, Z. Xia, M. Xu, Y. Lu and Z. Li, *Adv. Funct. Mater.*, 2018, **28**, 1706289.
5. B. Kumar, V. Atla, J. P. Brian, S. Kumari, T. Q. Nguyen, M. Sunkara and J. M. Spurgeon, *Angew. Chem. Int. Ed.*, 2017, **56**, 3645-3649.
6. H. Won da, C. H. Choi, J. Chung, M. W. Chung, E. H. Kim and S. I. Woo, *ChemSusChem*, 2015, **8**, 3092-3098.
7. R. Daiyan, X. Lu, W. H. Saputera, Y. H. Ng and R. Amal, *ACS Sustain. Chem. Eng.*, 2018, **6**, 1670-1679.
8. N. Han, Y. Wang, H. Yang, J. Deng, J. Wu, Y. Li and Y. Li, *Nat. Commun.*, 2018, **9**, 1320.
9. F. Lei, W. Liu, Y. Sun, J. Xu, K. Liu, L. Liang, T. Yao, B. Pan, S. Wei and Y. Xie, *Nat. Commun.*, 2016, **7**, 12697.
10. M.Watanabe, M.Shibata, A.Kato,M.Azuma, T.Sakata, *J. Electrochem. Soc.*, 1991,**138**, 3382-3389.
11. W. Luc, C. Collins, S. Wang, H. Xin, K. He, Y. Kang and F. Jiao, *J. Am. Chem. Soc.*, 2017, **139**, 1885-1893.
12. Y. Chen and M. W. Kanan, *J. Am. Chem. Soc.* , 2012, **134**, 1986-1989.
13. J.Wu, F.Risalvato, X.-D.Zhou, *ECS Trans*., 2012, **41**, 49-60.
14. S. Zhang, P. Kang and T. J. Meyer, *J. Am. Chem. Soc.*, 2014, **136**, 1734-1737.